Supporting Information: Synthesis of conjugated polymers by sustainable Suzuki polycondensation in water and under aerobic conditions

Alessandro Sanzone,[†] Adiel Calascibetta,[†] Mauro Monti,[†] Sara Mattiello,[†] Mauro Sassi,[†] Francesca Corsini,[‡] Gianmarco Griffini,[‡] Michael Sommer,[¶] and Luca Beverina[*,†]

†*Department of Materials Science, University of Milano-Bicocca, Via R. Cozzi, 55, 20125 Milano, Italy.*

‡*Department of Chemistry, Materials and Chemical Engineering "Giulio Natta", Politecnico di Milano, Piazza Leonardo da Vinci 32, 20133 Milano, Italy.*

¶*Institut for Chemistry, Chemnitz University of Technology, Straße der Nationen 62, 09111 Chemnitz, Germany.*

E-mail: luca.beverina@unimib.it

Contents

1 General

^{1}H NMR spectroscopy ^{1}H NMR spectra were recorded either using a Bruker Avance 400 NEO spectrometer (for PF8T2 samples) or at 500.13 MHz with a Bruker Avance III spectrometer using a 5 mm BBI gradient probe (for PF8BT samples). PF8T2 samples were measured at 80 °C, PF8BT samples were measured at 120 °C, $C_2D_2Cl_4$ was used as solvent and for calibration (δ (1H) = 5.98 ppm).

Uv-Vis spectroscopic analyses Evolution 600 UV-Vis spectrometer and VISION Pro software (both by Thermo Scientific) were used to collect and analyse data. Measurements were performed in air and at room temperature after the acquisition of a baseline which removes the contribution of air and of eventual contaminants.

FTIR spectra FTIR spectra were collected with a FT/IR-615 (Jasco Inc.) instrument used in transmission mode, at room temperature and in air. The number of scans performed was 64, the resolution 4 cm^{-1} and the range of the IR analyses was from 4000 cm^{-1} to 600 cm^{-1}.

Fluorescence spectroscopy Fluorescence spectra were acquired using a Jasco FP-6600 spectrofluorometer. The tests were carried out to measure both the emission and excitation spectra of the thin-film coatings.

DLS analysis Measurements were performed at room temperature on a 90Plus particle size analyzer (Brookhaven Instruments Corp.) with scattering angles of 15° and 90°, equipped with a 35 mW solid state 632.8 nm laser and a Brookhaven's TuboCorr correlator with 510 channels.

Profilometry Measurements were carried out with a KLA Tencor P-15 stylus profilometer.

SEC analysis Number-average (M_n) and weight-average (M_w) molecular weights were determined by size exclusion chromatography (SEC) and calibrated against polystyrene.

Samples of PF8T2 (entries 1 to 5 in Table 1) and PF8BT (entries 6 and 8 in Table 1) were measured at 35 °C on a Waters 510 HPLC system equipped with a Waters 2410 refractive index detector. THF was used as eluent. The sample to analyze (volume 200 µL, concentration in THF 2 mg/mL) was injected into a system of columns connected in series (Ultrastyragel models HR 4, HR 3, and HR 2, Waters), and the analysis was performed at a flow rate of 0.5 mL/min.

Samples of PF8BT (entries 6 to 9 in Table 1) were measured on four MZ-Gel SDplus 10E4 Å 5 µm columns with pore sizes ranging from 10^3 to 10^6 Å (Polymer Standards), connected in series with a RID-20A RI detector and a SPD-20AV UV detector (Shimadzu). THF was used as eluent at 40 °C with a flow rate of 1.0 mL/min.

2 Materials

All reagents and chemical compounds were purchased from Aldrich, Fluorochem, or TCI Europe and used without any further purification.

3 Optimization of formulative conditions on a model small molecule compound

Micellar catalyzed reactions are very resourceful but qualitatively different from corresponding transformations carried out in homogeneous phase. As the reaction requires colocalization of counterparts and catalysts within the same pocket of a micro heterogeneous mixture, the hydrophobic/hydrophilic balance and diffusion coefficients of all species are at least as important as the intrinsic reactivity. Table S1 shows all the results of our optimization study on the model reactions between 2,7-dibromofluorene (1) and thienyl-2-boronic acid (2) as well as on the same counterparts but with reversed functionalities, fluorene-2,7-diboronic acid (3) and 2-bromothiophene (4). Entries 1-3 show that the increase of the surfactant concentration from the customary 2 wt% to 10 and even 15 wt% does not improve conversion. It is also noticeable that the conditions we previously optimized for anthracene and isoindigo disubstituted symmetric derivatives work poorly in this case.[S1] Entries 4-6 show that the increase in the concentration of the organic base has a profound effect on both conversion and product distribution. The GC-MS yield evolves from 66% to 84%, 91% and eventually 93% upon increase of the amine stoichiometry from 3, to 6, 8 and 12 equivalents. From the standpoint of the reaction mechanism, such an excess of base should not influence the reaction behavior. The main impact of the amount of NEt_3 is in the nature of the formulation achieved: the amine acts as an organic cosolvent, thus helping in partially dissolving the lipophilic reagents.[S2] The concentration of the monoarylated species decreases accordingly. Thiophene-thiophene homocoupling is not observed when more than six equivalents on NEt_3 are employed. Entries 7 and 8 show the expected improvement of conversion and yield upon increase of the catalyst loading. In entry 9 we slightly reduced the Hydrophilic/Lipophilic Balance (HLB) of the surfactant system by mixing K-EL (HLB 13.5) with Span 80 (4.3). We recently demonstrated that the resulting mixture (HLB 10.7) is better suited to work with conjugated

Donor-Acceptor structures.[S3] Entry 10 shows that increase of the reaction temperature from 25 (entry 9) to 40 °C has a negligible impact on conversion and yield. Entry 11 confirms that carrying out the reaction under nitrogen atmosphere does not impact on yield or product distribution. Finally, we exchanged functionalities between reaction counterparts by using 2-bromothiphene and 9,9-dioctylfluorene-2,7-diboronic acid under the best conditions identified in the previous entries. Regardless the surfactant mixture (K-EL or K-EL/Span 80 7:3) we obtained quantitative conversion with 1% monoarylated species as the only discernible byproduct by GC-MS, in both cases working under standard laboratory atmosphere.

3.1 Experimental procedures

All reactions were carried out in a 5 mL CEM microwave glass tube vial under magnetic stirring at 1000 rpm and at a nominal concentration for fluorene derivative of 0.5 mol/L. Depending on the experiment, the surfactant concentration (Table S1, entries 1-3), the concentration of the organic base (entries 4-6), the catalyst loading (entries 7-8), the Hydrophilic/Lipophilic Balance (HLB) of the surfactant system (entry 9), the temperature (entry 10), the atmosphere (entry 11) and the functionalities between reaction counterparts (entries 12-13) vary. A representative experimental procedure for entry 4 is given as an example: 2,7-dibromo-9,9-dioctylfluorene (137 mg, 0.25 mmol), 2-thienylboronic acid (64 mg, 0.50 mmol) and Pd(dtbpf)Cl_2 (6.5 mg, 0.01 mmol) were weighed in the vial and then 0.5 mL of Kolliphor EL 2 wt% solution in water was added. The mixture was stirred and allowed to homogenize for 5 min before addition of the NEt_3 (152 mg, 1.50 mmol). All reactions were quenched after 12 h of stirring at room temperature, extracted with CH_2Cl_2, filtered over a pad of silica gel and submitted to GC-MS characterization. For entry 4 we proceeded with further purification of the product through column chromatography using a mixture of petroleum ether/CH_2Cl_2 (9:1) as eluent. The pure product was obtained in 80% yield (111 mg, 0.20 mmol).

Table S1: Optimization of reaction conditions in the coupling of dioctylfluorene and thiophene. All reactions were carried out in a 5 mL glass tube under magnetic stirring at 1000 rpm and at a nominal concentration for fluorene derivative of 0.5 mol/L. Worked up reaction mixtures were characterized by GC-MS using a simple semiquantitative area normalization method.

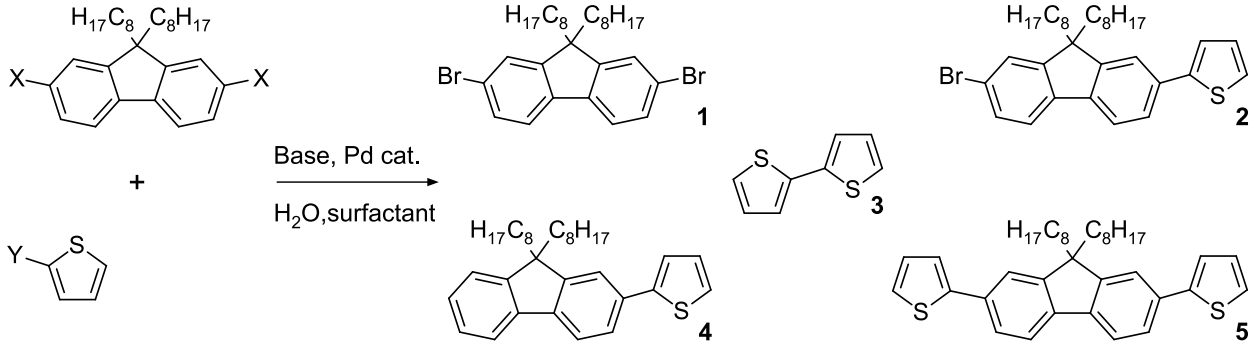

Entry	Medium (wt%)	X	Y	NEt_3 (eq)	[Pd][b] (mol%)	T (°C)	GC peak area (%)				
							1	2	3	4	5
1	K-EL (2)	Br	$B(OH)_2$	3	4	25	18	13	3	0	66
2	K-EL(10)	Br	$B(OH)_2$	3	4	25	38	11	3	0	48
3	K-EL(15)	Br	$B(OH)_2$	3	4	25	39	7	3	0	51
4	K-EL (2)	Br	$B(OH)_2$	6	4	25	8	6	2	0	84
5	K-EL (2)	Br	$B(OH)_2$	8	4	25	6	3	0	0	91
6	K-EL (2)	Br	$B(OH)_2$	12	4	25	6	1	0	0	93
7	K-EL (2)	Br	$B(OH)_2$	6	2	25	20	13	4	0	63
8	K-EL (2)	Br	$B(OH)_2$	6	8	25	5	1	1	0	93
9	K-EL/Span80 7/3 (2)	Br	$B(OH)_2$	6	4	25	3	2	1	0	94
10	K-EL/Span80 7/3 (2)	Br	$B(OH)_2$	6	4	40	2	2	1	0	95
11[a]	K-EL/Span80 7/3 (2)	Br	$B(OH)_2$	6	4	25	6	3	1	0	90
12	K-EL (2)	$B(OH)_2$	Br	6	4	25	0	0	0	1	99
13	K-EL/Span80 7/3 (2)	$B(OH)_2$	Br	6	4	25	0	0	0	1	99

[a] Under N_2 atmosphere. [b] Pd(dtbpf)Cl_2

4 Polymerization procedures

PF8T2 control sample The reaction was carried out according to literature conditions under inert atmosphere using Schlenck technique.[S4]

In a 50 mL two-necks round flask 5,5′-dibromo-2,2′-bithiophene (161.8 mg, 0.5 mmol) and 9,9-dioctylfluorene-2,7-diboronic acid (239.2 mg, 0.5 mmol) were dissolved in 11 mL of anhydrous toluene after three vacuum/N_2 cycles. Then 13 mg of the phase transfer catalyst, Aliquat 336 were added followed by 2 mL of 2 M aqueous NaOH. After the addition of $Pd(PPh_3)_4$ (5.8 mg, 0.005 mmol), the reaction mixture was stirred at 90 °C for 48 h. To provide defined end groups phenylboronic acid (137 mg, 2.2 eq), and after 2 h bromobenzene (176 mg, 2.2 eq) were added. After stirring for further 2 h the polymer was precipitated in methanol (60 mL), filtered and subsequently submitted to soxhlet extraction with MeOH, acetone, heptane and chloroform in order to remove the eccess of end-capping reagents, catalyst residues and oligomers. The polymer was obtained in 94.4% yield (261 mg, 0.472 mmol).

PF8BT control sample The reaction was carried out according to literature conditions under inert atmosphere using Schlenck technique.

In a 50 mL two-necks round flask 4,7-dibromo-2,1,3-benzothiadiazole (147.7 mg, 0.5 mmol) and 9,9-dioctylfluorene-2,7-diboronic acid pinacol ester (321.7 mg, 0.5 mmol) were dissolved in 3.6 mL of anhydrous toluene after three vacuum/N_2 cycles. Then 103 mg of the phase transfer catalyst, Aliquat 336 were added followed by 1.25 mL of 3.6 M aqueous K_2CO_3. After the addition of $Pd_2(dba)_3$ (4.6 mg, 0.005 mmol) and $P(o-tolyl)_3$ (3.4 mg, 0.0113 mmol), the reaction mixture was stirred at 90 °C for 48 h. To provide defined end groups phenylboronic acid (646 mg, 10.5 eq), and after 2 h bromobenzene (829 mg, 10.5 eq) were added. After stirring for further 2 h the reaction mixture was diluted with 8 mL of dichloromethane, filtered and subsequently precipitated in methanol (40 mL). Precipitated polymer was filtered and submitted to soxhlet extraction with MeOH, acetone,

heptane and chloroform in order to remove the eccess of end-capping reagents, catalyst residues and oligomers. The polymer was obtained in 89.6% yield (234 mg, 0.448 mmol).

General synthetic procedure for the optimization of the polymerization method in micellar and emulsion environment All the polymerizations were carried out in a 5 mL CEM microwave glass tube vial under magnetic stirring at 1000 rpm and at a nominal concentration for the monomers of 0.25 mol/L. Depending on the experiment, the medium and the temperature (table 1, entries 2-5 and 7-9) vary. A representative experimental procedure for entry 5 is given as an example:

9,9-dioctylfluorene-2,7-diboronic acid (239.2 mg, 0.5 mmol), 5,5′-dibromo-2,2′-bithiophene (162.0 mg, 0.5 mmol), and Pd(dtbpf)Cl_2 (13 mg, 0.02 mmol) were weighed in the vial and then 2 mL of Kolliphor EL 2 wt%/toluene 9:1 oil-in-water emulsion was added. The mixture was stirred and allowed to homogenize for 5 min at 80 °C, heating with an oil bath, before addition of the NEt_3 (304 mg, 3.0 mmol). After the addition of the base, the reaction mixture was stirred at 80 °C for 48 h. To provide defined end groups phenylboronic acid (183 mg, 3 eq), and after 2 h bromobenzene (157 mg, 3 eq) were added. After stirring for further 2 h the polymer was precipitated in methanol (10 mL) and then submitted to soxhlet extraction with MeOH, acetone, heptane and chloroform in order to remove the excess of end-capping groups, catalyst residues and oligomers. The polymer was obtained in 86.8% yield (240 mg, 0.434 mmol).

5 Analysis of the colloidal state of the reactions

To characterize the colloidal properties of the reactions mixtures, we performed DLS measurements of as prepared monomers dispersions both in K-EL 2% in water and K-EL 2% in water / toluene 9:1. The measurements could not be performed at the nominal reagents concentration used for the coupling reactions (0.5 M), as unreliable results were obtained. For this reason, the measurements were performed at 0.05 M nominal reagents concentration. Figure S1 shows the DLS analysis of mixtures obtained sonicating 9,9-dioctylfluorene-2,7-diboronic acid (12.0 mg), 5,5′-dibromo-2,2′-bithiophene (8.1 mg) and Et_3N (15 mg) in 1 mL of either K-EL 2% in water or K-EL 2% in water / toluene 9:1. As prepared K-EL 2% in water and K-EL 2% in water / toluene 9:1 are also added as comparison. The addition of the monomers turns the K-EL surfactant solution into a dispersion, with particles size in the micrometer range, the same observed for the toluene emulsions.

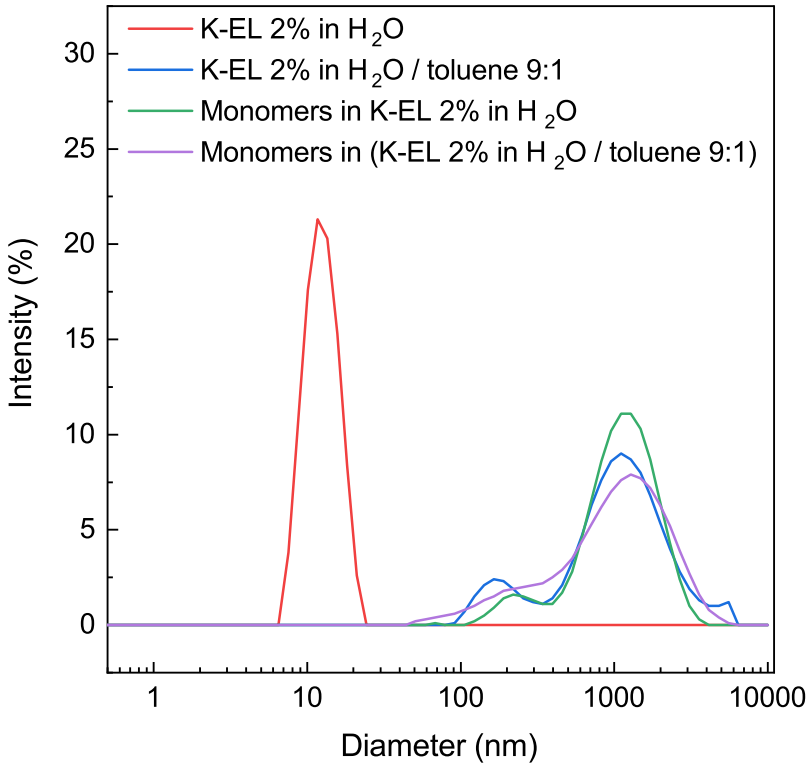

Figure S1: DLS analysis of K-EL 2% in water (red), K-EL 2% in water / toluene 9:1 (blue), and dispersions of 9,9-dioctylfluorene-2,7-diboronic acid and 5,5′-dibromo-2,2′-bithiophene in K-EL 2% in water (green) and K-EL 2% in water / toluene 9:1 (purple).

6 Polymerization statistics for PF8BT and PF8T2 reported in the literature

Table S2: Examples of polymerization statistics for PF8BT reported in the literature.

Entry	M_n (kg/mol)	M_w (kg/mol)	Đ	Ref.
1	9.4	21.6	2.3	Behrendt *et al.*[S5]
2	23.5	42.8	1.82	Liang *et al.*[S6]
3	18.7	38.0	2.03	Peng *et al.*[S7]
4	23.5	42.8	1.82	Wang *et al.*[S8]
5	5.03	8.95	1.78	Yu *et al.*[S9]
6	16.6	29.9	1.82	Zhou *et al.*[S10]

Table S3: Examples of polymerization statistics for PF8T2 reported in the literature.

Entry	M_n (kg/mol)	M_w (kg/mol)	Đ	Ref.
1	11	21	1.9	Rander and Leclerc[S11]
2	19	41	2.2	Morin *et al.*[S12]
3	29.2	138	4.73	Kettner *et al.*[S4]

7 Calculation of E_{factor} for literature and micellar polymerization procedures

As the reported reactions are palladium mediated C−C couplings, water has always been taken into account for the calculation of the E-factor. In fact, it can be contaminated with palladium, and it therefore must be considered an hazardous waste. For this reason, inorganic bases used in the reactions are included as well in the waste calculation, as they remain dissolved in the aqueous phase.

Solvents used for soxhlet extraction are not taken into account, as they were recovered by distillation at the end of the purification.

The E_{factor} is calculated as

$$E_{factor} = \frac{m_{reagents} + m_{solvents} - m_{product}}{m_{product}} = \frac{m_{waste}}{m_{product}}$$

The E_{factor} of each procedure excluding purification is reported as well to facilitate the comparison with the protocol for the preparation of polymer nanoparticles (which does not include purification).

Synthesis of PF8T2 in homogeneous reaction medium

Table S4: PF8T2 control sample (table 1, entry 1).

	n (mmol)	mass (g)	volume (mL)	density ($g\,mL^{-1}$)
9,9-dioctylfluorene-2,7-diboronic acid	0.5	0.2392		
5,5′-dibromo-2,2′-bithiophene	0.5	0.1618		
NaOH 2 M in H_2O	4	2.16	2.00	1.08
$Pd(PPh_3)_4$	0.005	0.0058		
Aliquat 336		0.013		
toluene		9.537	11	0.867
Termination and purification				
phenylboronic acid		0.137		
bromobenzene		0.176		
methanol		47.52	60	0.792
PF8T2	0.472	0.261		
Waste and E_{factor}				
Waste (purification excluded): 11.8558 g. $E_{factor} = 45.4$				
Waste (purification included): 59.6888 g. $E_{factor} = 229$				

Synthesis of PF8T2 in micellar conditions

Table S5: PF8T2 sample obtained under micellar conditions (table 1, entry 5).

	n (mmol)	mass (g)	volume (mL)	density ($g\,mL^{-1}$)
9,9-dioctylfluorene-2,7-diboronic acid	0.5	0.2392		
5,5′-dibromo-2,2′-bithiophene	0.5	0.1620		
NEt_3	3.0	0.304		
$Pd(dtbpf)Cl_2$	0.02	0.0130		
Kolliphor EL 2 wt% in water		1.8	1.8	1.0
toluene		0.173	0.2	0.867
Termination and purification				
phenylboronic acid		0.183		
bromobenzene		0.157		
methanol		7.92	10	0.792
PF8T2	0.434	0.240		
Waste and E_{factor}				
Waste (purification excluded): 2.4512 g. $E_{factor} = 10.2$				
Waste (purification included): 10.7112 g. $E_{factor} = 44.6$				

Synthesis of PF8T2 nanoparticles in miniemulsion

Table S6: Literature protocol described by Turner *et al.* (*Macromolecules* 2014, 47, 19, 6531-6539; table 1, reaction J).[S13] PF8T2 was not isolated after synthesis, therefore the amount of product obtainable from quantitative reaction conversion was used to estimate the E_{factor}.

	n (mmol)	mass (g)	volume (mL)	density ($g\,mL^{-1}$)
9,9-dioctylfluorene-2,7-diboronic acid bis(1,3-propanediol) ester	0.8	0.4467		
5,5′-dibromo-2,2′-bithiophene	0.8	0.2592		
$N(Et)_4OH$ 40% in H_2O	1.6	0.320		
(IPr*)$PdCl_2$(TEA)	0.032	0.0382		
Triton X-102		5.0		
xylene		3.456	4.00	0.864
H_2O		45	45.0	1.00
PF8T2	0.8	0.442		
Waste and E_{factor}				
Waste (purification excluded): 54.0781 g. $E_{factor} = 122$				

This protocol was reported to clarify that it serves as a method to prepare nanoparticles of the semiconducting polymer. A large amount of water and surfactant is needed to form the miniemulsion (water to product ratio is around 102, surfactant to product ratio is around 11). The protocol is optimized to obtain a precise particles morphology, and the aqueous reaction medium, which accounts for 92% of the waste, serves also as dispersing medium for the particles. This is not the case of the micellar protocol described in this paper, which uses aqueous surfactant solution only as the reaction medium to synthesize amorphous polymer powder (water to product ratio is around 7.4, surfactant to product ratio is 0.15).

Synthesis of PF8BT in homogeneous reaction medium

Table S7: PF8BT control sample (table 1, entry 6)

	n (mmol)	mass (g)	volume (mL)	density ($g\,mL^{-1}$)
9,9-dioctylfluorene-2,7-diboronic acid pinacol ester	0.5	0.3217		
4,7-dibromo-2,1,3-benzothiadiazole	0.5	0.1477		
K_2CO_3 3.6 M in H_2O	4.5	1.725	1.25	1.38
$Pd_2(dba)_3$	0.005	0.0046		
$P(o-tolyl)_3$	0.0113	0.0034		
Aliquat 336		0.103		
toluene		3.12	3.6	0.867
Termination and purification				
phenylboronic acid		0.646		
bromobenzene		0.829		
DCM		10.64	8	1.33
methanol		31.68	40	0.792
PF8BT	0.448	0.234		
Waste and E_{factor}				
Waste (purification excluded): 5.1914 g. $E_{factor} = 22.2$				
Waste (purification included): 48.9864 g. $E_{factor} = 209$				

Synthesis of PF8BT in micellar conditions

Table S8: PF8BT sample obtained under micellar conditions (table 1, entry 9)

	n (mmol)	mass (g)	volume (mL)	density ($g\,mL^{-1}$)
9,9-dioctylfluorene-2,7-diboronic acid	0.5	0.2392		
4,7-dibromo-2,1,3-benzothiadiazole	0.5	0.1470		
NEt_3	3.0	0.304		
$Pd(dtbpf)Cl_2$	0.02	0.0130		
Kolliphor EL 2 wt% in water		1.8	1.8	1.0
toluene		0.173	0.2	0.867
Termination and purification				
phenylboronic acid		0.183		
bromobenzene		0.157		
methanol		7.92	10	0.792
PF8BT	0.450	0.235		
Waste and E_{factor}				
Waste (purification excluded): 2.4412 g. $E_{factor} = 10.4$				
Waste (purification included): 10.7012 g. $E_{factor} = 45.5$				

Synthesis of PF8BT nanoparticles in miniemulsion

Table S9: Literature protocol described by Turner *et al.* (*Macromolecules* 2014, 47, 19, 6531-6539; table 1, reaction F).[S13] PF8BT was not isolated after synthesis, therefore the amount of product obtainable from quantitative reaction conversion was used to estimate the E_{factor}.

	n (mmol)	mass (g)	volume (mL)	density ($g\,mL^{-1}$)
9,9-dioctylfluorene-2,7-diboronic acid bis(1,3-propanediol) ester	0.4	0.2234		
4,7-dibromo-2,1,3-benzothiadiazole	0.4	0.1176		
$N(Et)_4OH$ 40% in H_2O	0.8	0.160		
(IPr*)$PdCl_2$(TEA)	0.016	0.0191		
Triton X-102		2.5		
xylene		1.728	2.00	0.864
H_2O		47.5	47.5	1.00
PF8BT	0.4	0.209		
Waste and E_{factor}				
Waste (purification excluded): 52.0391 g. $E_{factor} = 249$				

This protocol was reported to clarify that it serves as a method to prepare nanoparticles of the semiconducting polymer. A large amount of water and surfactant is therefore needed to form the miniemulsion (water to product ratio is nearly 230, surfactant to product ratio is around 12). The protocol is optimized to obtain a precise particles morphology, and the aqueous reaction medium, which accounts for 96% of the waste, serves also as dispersing medium for the particles. This is not the case of the micellar protocol described in this paper, which uses aqueous surfactant solution only as the reaction medium to synthesize amorphous polymer powder (water to product ratio is around 7.5, surfactant to product ratio is around 0.15).

8 Evaluation of the emission efficiency and photostability of emulsion *vs.* homogeneous phase polymerized materials

8.1 Coatings preparation

PF8T2 samples (Table 1 entries 1 and 5) and PF8BT samples (Table 1 entries 6 and 8) were spin coated (800 rpm, 60 s) from $CHCl_3$ solutions (15 mg/mL) on glass or quartz slides using a Laurell WS-400BZ-6NPP/LITE instrument.

8.2 Comparative photostability tests

We submitted the best samples obtained via emulsion approaches to comparative luminescence and photostability tests with respect to the samples obtained via the literature approach. We selected Table 1 entry 5 sample as the representative emulsion polymerized PF8T2 and Entry 8 sample as the representative PF8BT sample. We submitted both polymers, along with the corresponding control experiment samples (Table 1 entry 1 for PF8T2 and Entry 6 for PF8BT) to extended photostability tests.

We characterized each sample under three different exposition conditions:

a) accelerated weathering tests in a weather-o-meter chamber, equipped with a white-light Xenon lamp and outdoor filter, able to cut out all the wavelengths lower than 280 nm. The total irradiance applied was equal to 550 W/m^2 in the 300-800 nm wavelength range, the temperature was fixed at 35 °C and the relative humidity at 25%;

b) UV-A accelerated weathering tests in air, performed using a UV polymerization apparatus (Helios Quartz, POLIMER 400W) equipped with a high-pressure mercury UV-A lamp (Zs type, Helios Quartz) characterized by an emission window between

315 and 400 nm and with radiative power density equal to 300 W/m^2;

c) the same test described in b) was repeated under N_2 atmosphere.

8.2.1 PF8T2 samples

Weathering test under white-light in air Figure S2 shows the behavior of PF8T2 spin coated films under white-light irradiation. The thicknesses of the two samples are comparable (351 nm for Table 1 entry 1 sample and 353 nm for Table 1 entry 5 sample). The degradation kinetics is essentially indistinguishable for the two samples both from the standpoint of absorption profiles (Figure S2a and S2b) and luminescence spectra (Figure S2c and S2d). Specifically, within 1h the fluorescence intensity of both the samples sharply drops: a reduction of 94% and 93% in the fluorescence intensity has been recorded for entry 1 and 1ntry 5, respectively. Simultaneously, a decrease in the maximum absorption values (13% for entry 1 and 15% for entry 5) has been detected. Subsequently, a progressive decrease in absorbance and fluorescence intensity has been verified. After 6 h, the maximum absorbance of entry 1 and entry 5 reaches values equal to $\sim$28 % and $\sim$20 % of the initial maximum absorbance, respectively. Whereas, the maximum fluorescence intensity of both samples reaches values equal to $\sim$2.5 % the initial one. The lack of photostability of fluorene containing polymers is well established in the literature and we did not expect our samples to be any different.[S14,S15] It is however clear that the micellar catalyzed polymerization technique does not influence the degradation kinetics. The almost immediate quanching of the fluorescence signal is ascribed to the formation of fluorenone quenching sites. It is however worthwhile noting that the initial luminescence intensity of the two samples is almost the same. As the thicknesses are also essentially identical, it is possible to conclude that the emission efficiency of the two polymers is also similar. Actually, the emulsion polymerized sample is around 10% more efficient that the control sample.

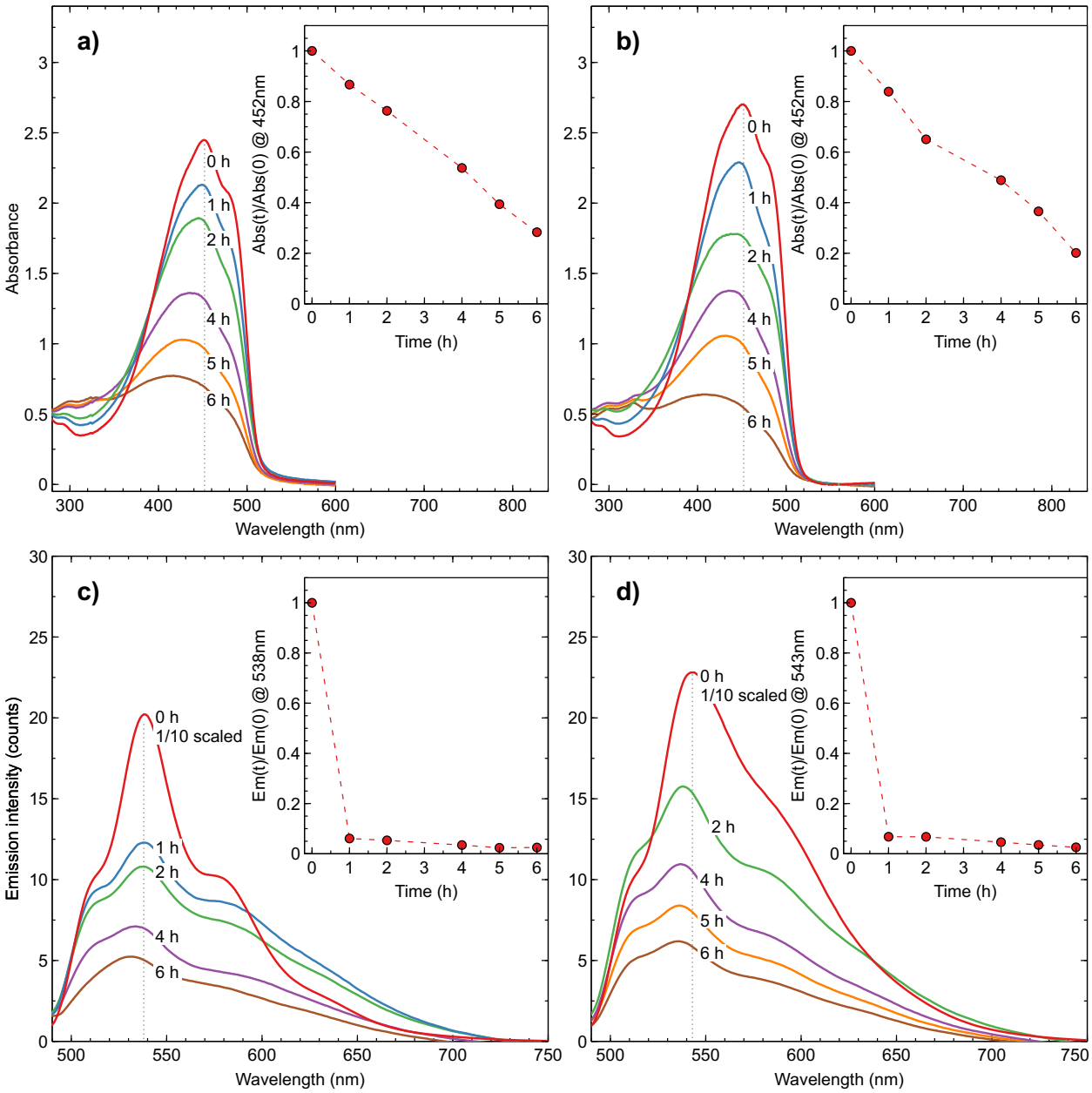

Figure S2: UV-Vis absorption (top) and steady state emission spectra under excitation at 485 nm (bottom) as the function of the irradiation time (white-light) for spin coated thin films of of PF8T2 samples: Table 1 Entry 1 (a and c) and Table 1 Entry 5 (b and d). Emission spectra at 0 h were scaled to 1/10.

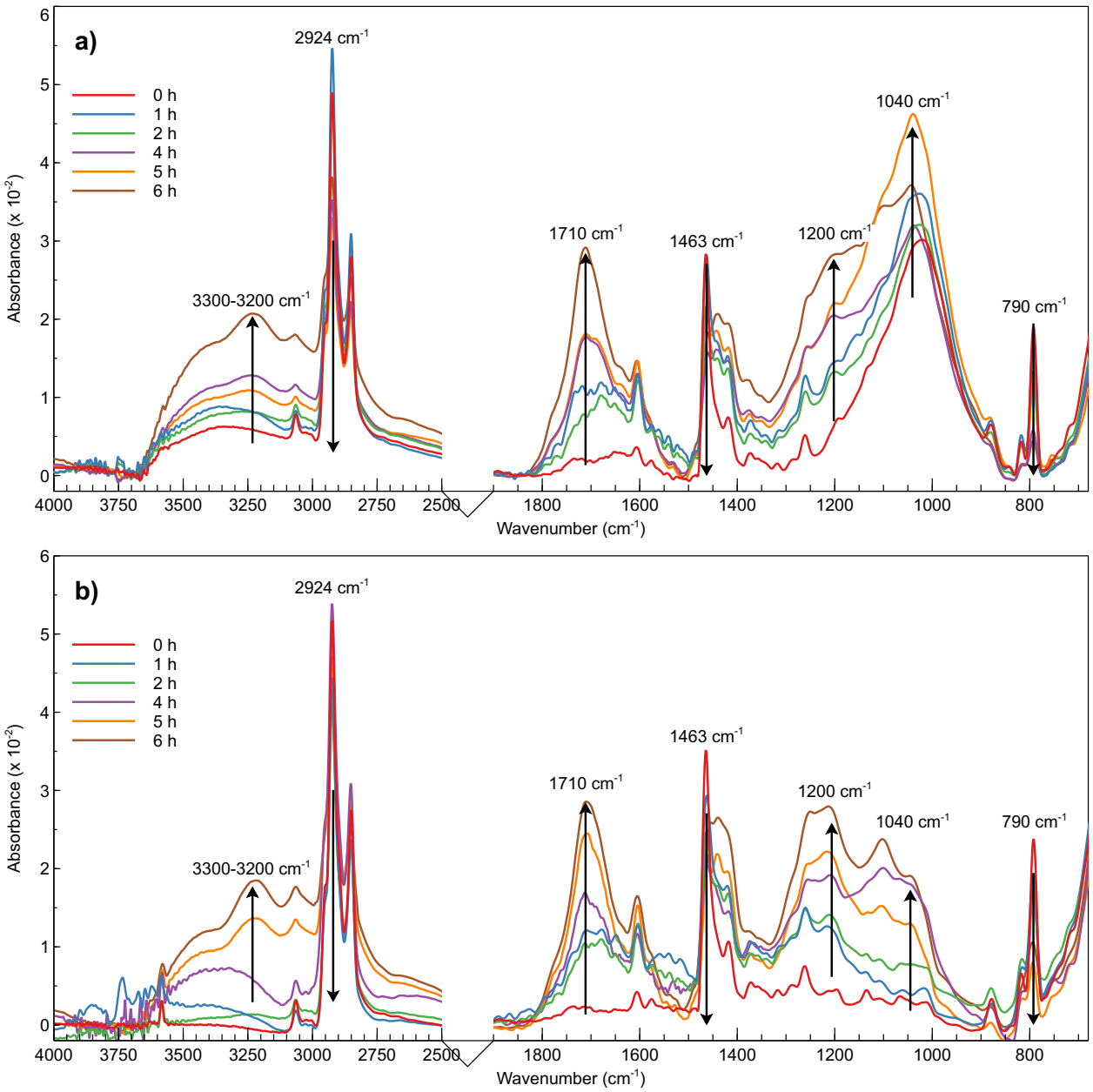

Figure S3: FTIR spectra as a function of the irradiation time (white-light) of spin coated thin films of PF8T2 samples: control experiment (Table 1 Entry 1) (a) and emulsion polymerized (Table 1 Entry 5) (b).

We carried out a comparative FTIR study to verify that the mechanism of degradation is the same for both samples. Figure S3 shows similar features for both samples. Indeed, the spectra of both the samples show a progressive disappearance of the absorption bands attributed to alkyl groups connected with the oxidation of the fluorene residue to fluorenone.[S15,S16] Specifically, a reduction in intensity at 2924 cm^{-1} and 2850 cm^{-1} related to the stretching of saturated C−H groups, at 1463 cm^{-1} due to C−H bending and C=C stretching vibration of the ring structure, and at 790 cm^{-1} associated to C−H rocking has been observed. Such decrease of intensity for signals attributed to alkyl groups is accompanied by the appearance of new bands at 1710 cm^{-1}, attributed to carbonyl species. Both spectra also show a progressive increase in the intensity of the peak related to sulfoxides and sulfones S=O stretching (1040 cm^{-1} and 1200 cm^{-1} respectively) diagnostics of the oxidation of the thiophene repeating units.[S17] The only minor difference between the two spectra is associated with the sulfoxide peak at 1040 cm^{-1}, already evident at time 0 for the control experiment while sizably weaker for the emulsion polymerized one.
Comparison of profilometric measurements before and after 6 h of irradiation do not reveal any significant variation in films thickness (Table S10). The exposed films were also dissolved in THF and the SEC characterization was performed and compared with data of the pristine sample. Table S10 shows that in both cases the light exposure causes a slight decrease in the molecular weight and a corresponding increase in dispersity. The behavior is very similar for the two samples. This results indicate that photo-oxidation likely leads to chain scission.

UVA Weathering test in air We thus repeated the weathering test using a UV-A light source under air and under nitrogen to ascertain that the light sensitivity of both samples is connected with high energy irradiation and that the process is oxygen mediated.
UV-Vis and fluorescence spectroscopy analyses again show similar degradation rates of

Table S10: GPC polymerization statistics and profilometric thickness for PF8T2 films before and after weathering for 6 h under white-light irradiation

Sample	Weathered	M_n (kg/mol)	Đ	Thickness (nm)
Control[a]	No	24.2	1.64	350.6 ± 19.4
	Yes 💡	18.1	1.99	334.7 ± 21.5
Emulsion[b]	No	25.2	1.96	352.6 ± 9.4
	Yes 💡	18.2	2.23	340.3 ± 13.3

[a] Entry 1 of Table 1 (Toluene).
[b] Entry 5 of Table 1 (K-EL/Tol. 9:1).

both entries 1 and 5 in Table 1. If compared with the results obtained from accelerated weathering tests under white-light, a similar degradation of both the samples can be noticed (Figure S4). Within 1 h, a reduction of the fluorescence intensity by ∼81 % and ∼78 % has been detected for entry 1 and entry 5, respectively. At the same time, a reduction in the maximum absorption values (12 % for 1 and 5.5 % for 5) has been recorded. Moreover, after 6 h, the maximum absorbance of entries 1 and 5 reaches values equal to 47 % and 55 % of the initial maximum absorbance, respectively. For what concerns the values of maximum fluorescence intensity, they have been found to decrease down to 8 % and 10 % of the original one for entries 1 and 5, respectively.

The IR spectra of the samples during UV-A exposure in air (Figure S5) display similar modifications to those detected in the samples aged with accelerated weathering tests under white-light irradiation, thus further demonstrating that UV-induced photooxidation can be considered as the main degradation mechanism occurring in the material. A smaller variation in the intensity of the peaks from their original value can be noticed, which could be related to a slightly slower degradation rate resulting from the lower value of total irradiance (and narrower emission spectral window in the UV) to which the samples have been exposed.

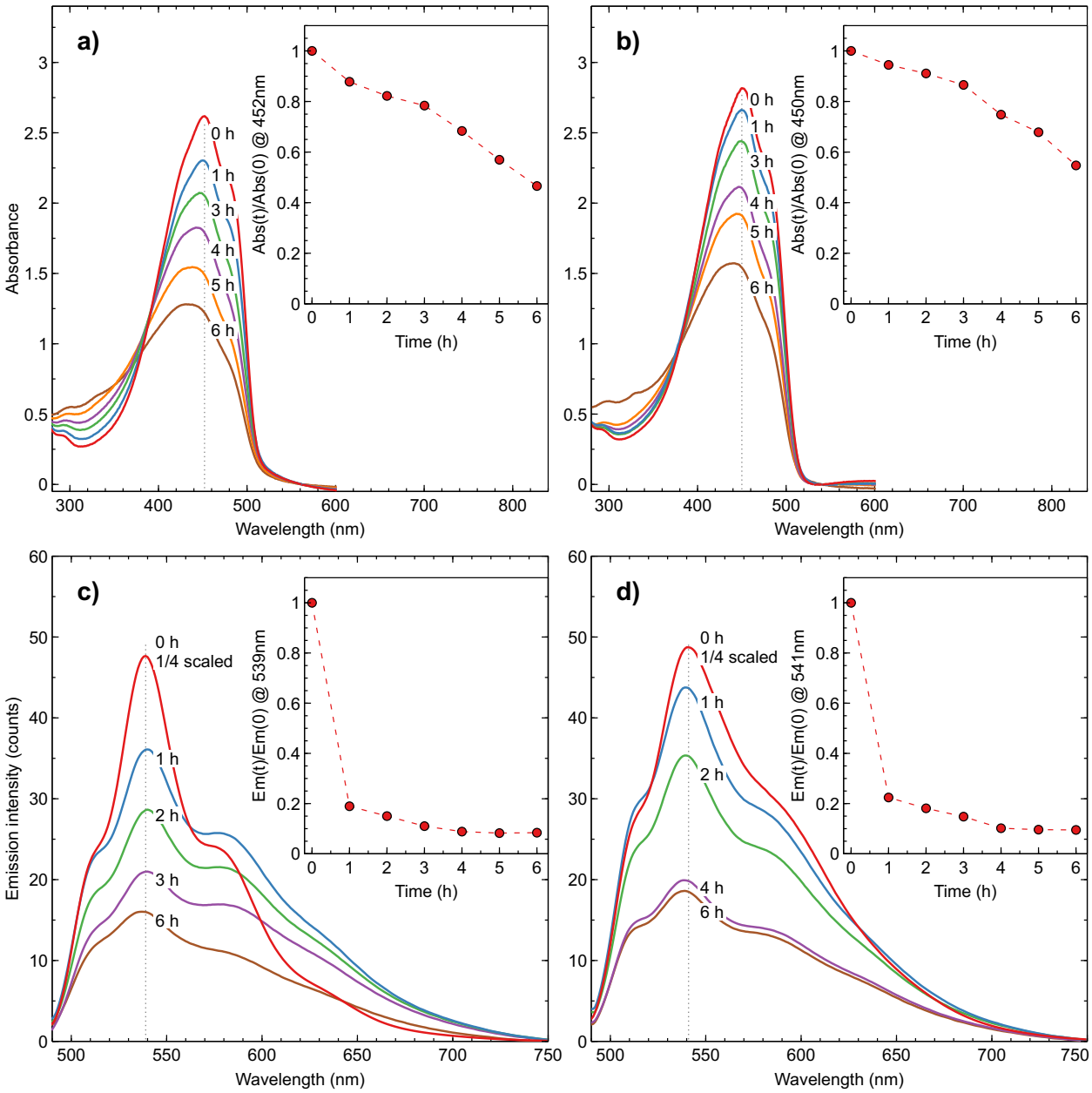

Figure S4: UV-Vis absorption (top) and steady state emission spectra under excitation at 485 nm (bottom) as the function of the irradiation time (UVA light, air) for spin coated thin films of of PF8T2 samples: Table 1 Entry 1 (a and c) and Table 1 Entry 5 (b and d). Emission spectra at 0 h were scaled to 1/4.

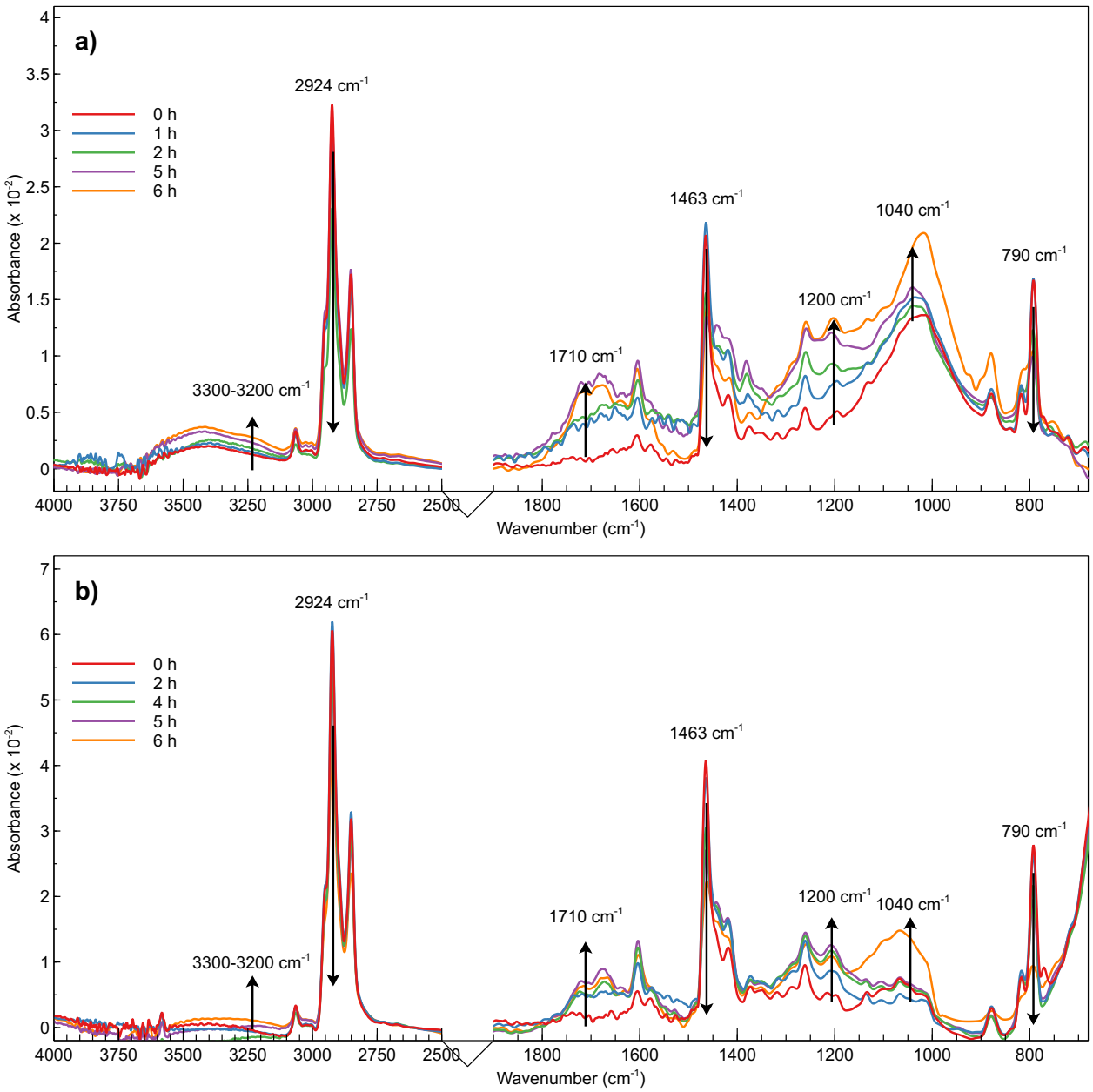

Figure S5: FTIR spectra as a function of the irradiation time (UVA light, air) of spin coated thin films of PF8T2 samples: control experiment (Table 1 Entry 1) (a) and emulsion polymerized (Table 1 Entry 5) (b).

UVA Weathering test in inert (N_2) atmosphere As previously stated, with the purpose of assessing the influence of oxygen present in air atmosphere on the degradation rate, irradiation tests under UV-A light ($300\,W/m^2$) were repeated in inert (N_2) atmosphere. The UV-Vis and fluorescence spectra (Figure S6) show comparable and very small degradation rates of both entry 1 and entry 5 of Table 1. After 1 h of testing, no relevant reduction in the maximum absorbance values has been detected, whereas entries 1 and 5 retain $\sim$83 % and $\sim$67 % of their original value of fluorescence intensity. Even after 6 h, the maximum absorbance of entry 1 and entry 5 decreases of only $\sim$4 %. Instead, the values of maximum fluorescence intensity reach values equal to $\sim$50 % and $\sim$42 % with respect to their initial values. These values are remarkably higher with respect to those achieved with the previous two testing protocols.

No significant spectral modifications have been evidenced from the IR monitoring (Figure S7) of both the samples during UV-A irradiation in nitrogen atmosphere.

The results of UV-Vis, fluorescence and FTIR spectroscopic analyses conducted on PF8T2 samples to monitor the degradation path during irradiation to UV-A light in inert and non-inert atmosphere clearly demonstrate that the degradation of the samples took place more rapidly in the presence of air. This suggests that the main phenomenon responsible for the deterioration of the chemical and physical properties of both materials is photooxidation, although some photolytic processes seem to have occurred as well, as evident by the slight variations observed from UV-Vis, fluorescence and FTIR spectra of both materials in inert atmosphere. Moreover, the degradation rate of the two samples has been demonstrated to be comparable.

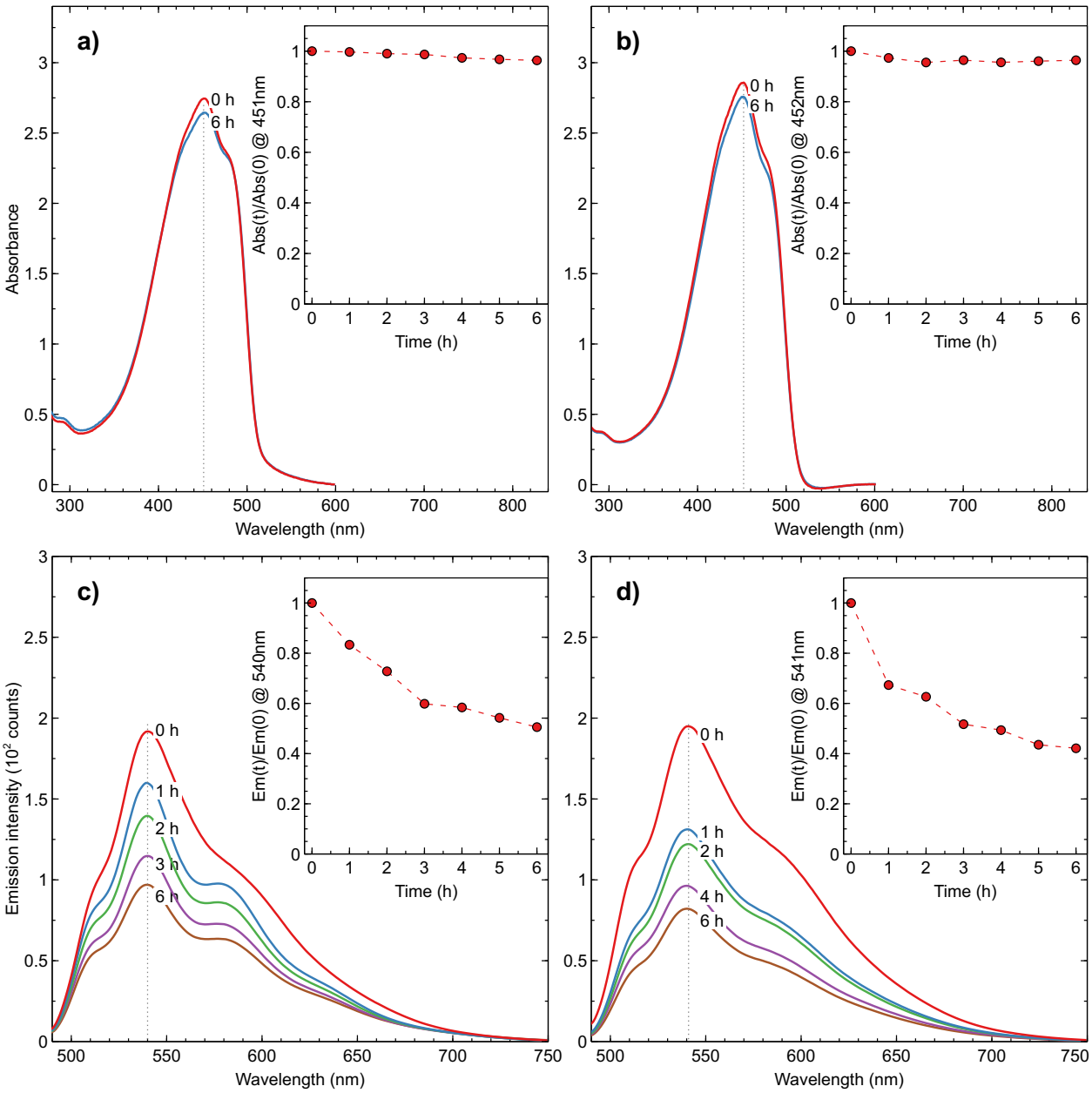

Figure S6: UV-Vis absorption (top) and steady state emission spectra under excitation at 485 nm (bottom) as the function of the irradiation time (UVA light, N_2) for spin coated thin films of of PF8T2 samples: Table 1 Entry 1 (a and c) and Table 1 Entry 5 (b and d).

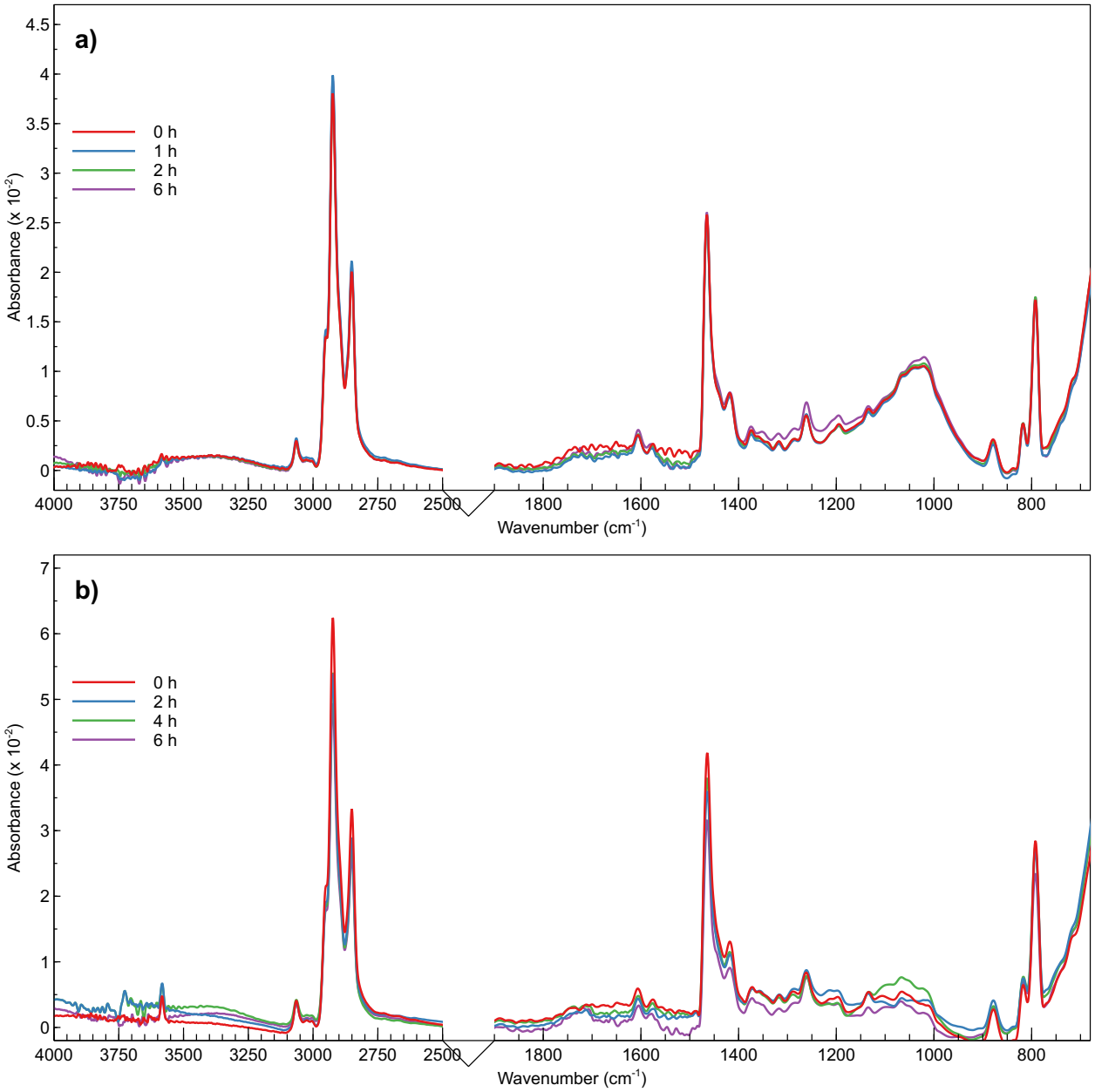

Figure S7: FTIR spectra as a function of the irradiation time (UVA light, N_2) of spin coated thin films of PF8T2 samples: control experiment (Table 1 Entry 1) (a) and emulsion polymerized (Table 1 Entry 5) (b).

8.2.2 PF8BT samples

Weathering test under white-light in air We performed the same comparative tests on PF8BT samples, with slightly different results. Figure S8 shows that in this case the degradation kinetics for the two samples under white-light irradiation have similar characteristics but they are not identical. In both cases, the charge transfer band is progressively bleached in intensity and slightly blue-shifted. However, in the case of the control sample (Table 1 entry 6) the intensity at the low-energy maximum after 20 h of exposure is 10 % of the initial value (Figure S8a), whereas for the emulsion polymerized sample (Table 1 entry 8) the absorption spectrum retains 43 % of the original intensity (Figure S8b)). The steady state emission spectra show a similar trend: the emission intensity progressively drops for both polymers but the emulsion polymerized sample (Figure S8d) retains 34 % of the original efficiency whereas the control sample (Figure S8c) only retains 10 %. As in the previous case, both sample thicknesses (281 nm for Table 1 entry 6 sample and 295 nm for Table 1 entry 8 sample) and initial emission intensities are comparable.

Significant modifications of the IR spectra of the polymer have been observed, from which photo-oxidation appears to be the most likely degradation mechanism (Figure S9). A progressive reduction of absorption intensity was observed for various functional groups. In particular, the intensity of the absorption bands related to alkyl groups (2924 cm^{-1} and 2850 cm^{-1} related to the stretching of saturated C−H groups, at 1463 cm^{-1} due to C−H bending and C=C stretching vibration of the ring structure), aromatic C−H (3055 cm^{-1}) and 1,2,5-thiadiazole ring (806 cm^{-1} ring in-plane bending) rapidly decreased. The peak at 806 cm^{-1} could also correspond to the in-plane bending vibration of the alkyl side chain in the fluorene unit, that is considered to decompose and oxidize through light irradiation, resulting in a molecular structure variation from fluorene to fluorenone and a consequent reduction in the peak intensity.[S16,S18] In addition to the aforementioned trends, the simultaneous appearance of other absorption bands has been noticed. Several features appeared in the carbonyl region (1710 cm^{-1}). Also, an increase in the intensity

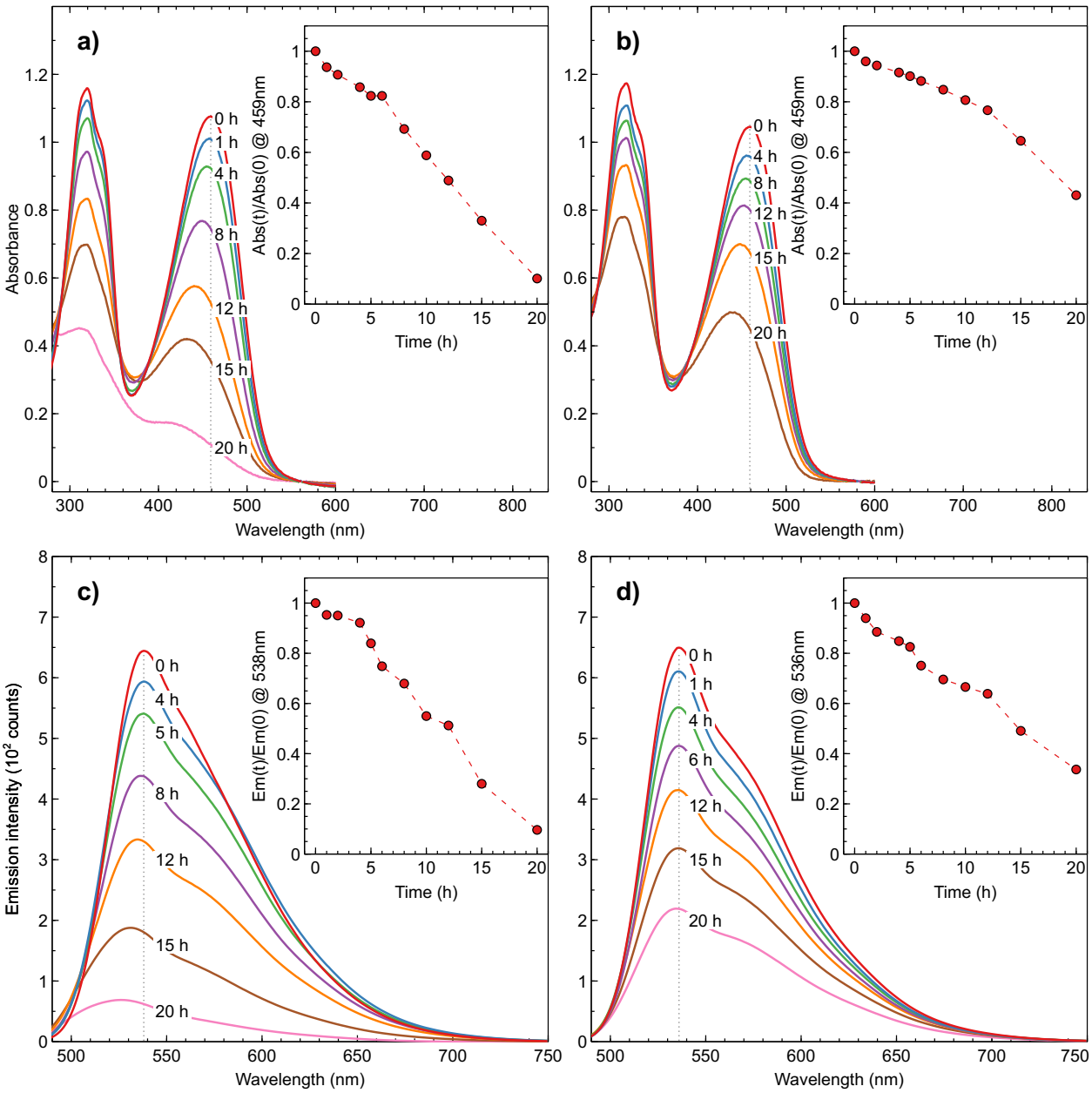

Figure S8: UV-Vis absorption (top) and steady state emission spectra under excitation at 450 nm (bottom) as the function of the irradiation time (white-light) for spin coated thin films of of PF8BT samples: Table 1 Entry 6 (a and c) and Table 1 Entry 8 (b and d).

of the −OH stretching peak (∼3300 cm^{-1}) has been detected. Spectral variations in the region between 1000 cm^{-1} and 1350 cm^{-1} might be due to formation of sulphone and sufoxide groups S=O by oxidation of 2,1,3-benzothiadiazole units.[S19] In general, more visible modifications in the FTIR spectra were detected in entry 6 than in entry 8.

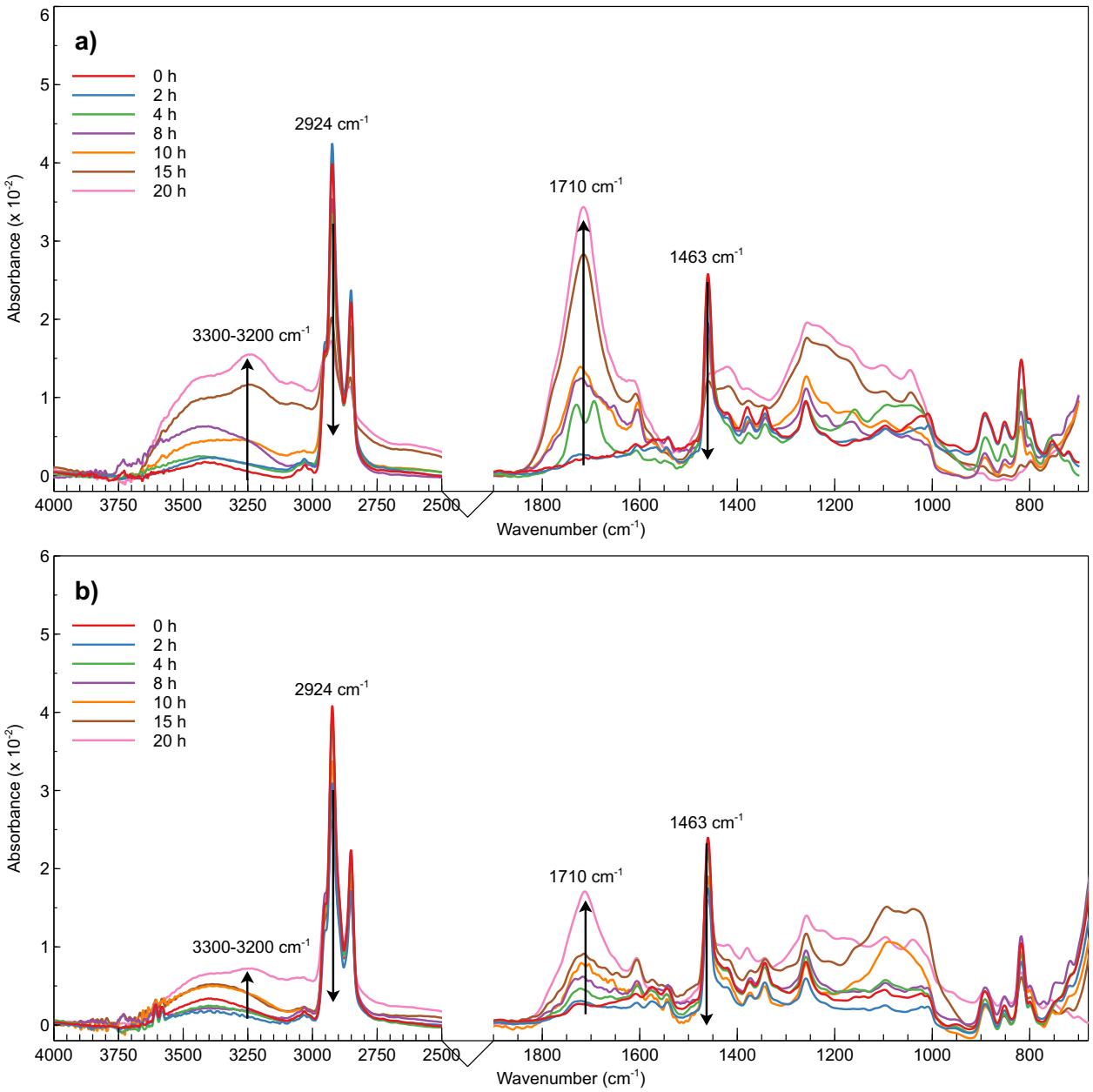

Figure S9: FTIR spectra as a function of the irradiation time (white-light) of spin coated thin films of PF8BT samples: control experiment (Table 1 Entry 6) (a) and emulsion polymerized (Table 1 Entry 8) (b).

From SEC data of both samples (Table S11), it can be noticed that after aging the original high molecular weight peak shifts towards longer retention times (lower molecular weights). This indicates that photo-oxidation leads to random chain scission of the molecule and to a broadening of the molecular weight distribution. The process of chain

scission takes place quite rapidly since the molecular weight of both entry 6 and entry 8 decreases by ∼21 % in 20 h of exposure. No significant changes in the coatings thickness have been detected by profilometric measurements.

Table S11: GPC polymerization statistics and profilometric thickness for PF8BT films before and after weathering for 20 h under white-light irradiation

Sample	Weathered	M_n (kg/mol)	Đ	Thickness (nm)
Control[a]	No	10.1	2.07	281.3 ± 9.7
	Yes	8.06	2.34	274.6 ± 10.1
Emulsion[b]	No	18.5	2.03	294.7 ± 10.4
	Yes	14.6	2.56	290.7 ± 11.9

[a] Entry 6 of Table 1 (Toluene).
[b] Entry 8 of Table 1 (K-EL/Tol. 9:1).

UVA Weathering test in air The effect of the UV-A component of the solar radiation on the degradation rate was again evaluated through irradiation tests with UV-A light ($300\,W/m^2$) in non-inert (air) atmosphere. UV-Vis and fluorescence spectroscopic analyses show similar degradation rates for both the samples (Figure S10). If compared with the results obtained from the samples treated with accelerated weathering tests under white-light irradiation (Figure S8), a slightly slower decline in the maximum fluorescence intensity is observed. Indeed, after 6 h the maximum fluorescence intensity for entries 6 and 8 reaches values equal to ∼82 % and ∼83 % of the original one, whereas values equal to ∼75 % of the original ones have been obtained in the accelerated weathering tests under white-light. This could be due to the lower value of total irradiance (and narrower spectral range in the UV) used during testing.

FTIR spectroscopic analysis (Figure S11) show similar spectral modifications to those reported for photo-oxidation under white-light irradiation. Also, a comparable variation in the intensity of the peaks from their original value can be observed.

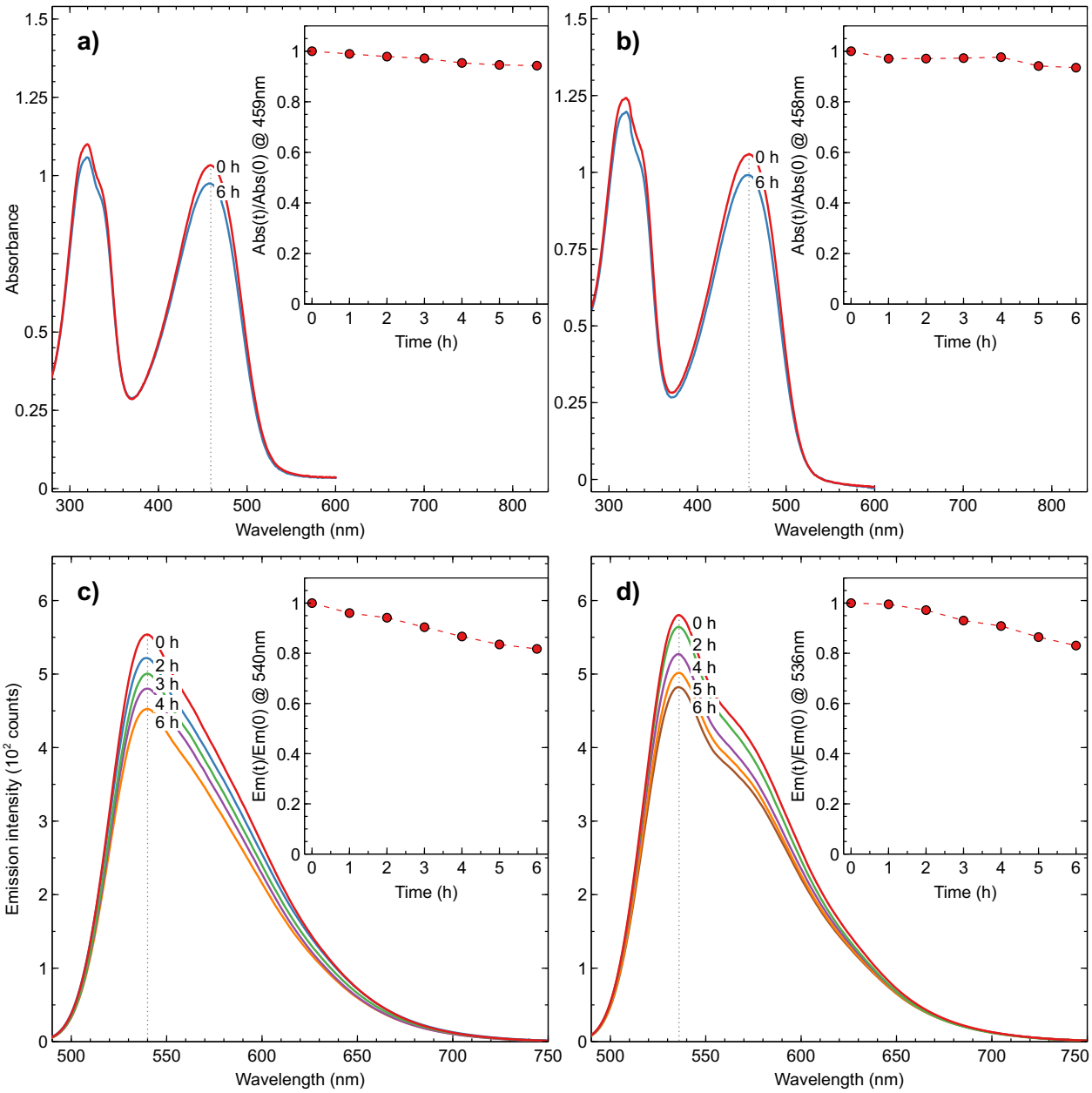

Figure S10: UV-Vis absorption (top) and steady state emission spectra under excitation at 450 nm (bottom) as the function of the irradiation time (UVA light, air) for spin coated thin films of of PF8BT samples: Table 1 Entry 6 (a and c) and Table 1 Entry 8 (b and d).

UVA Weathering test in inert (N_2) atmosphere The impact of oxygen on the degradation rate and mechanism was investigated comparing the previous results with those obtained through irradiation under UV-A light (300 W/m^2) in inert (N_2) atmosphere. The UV-Vis spectra (Figure S12) show that both samples do not undergo significant degra-

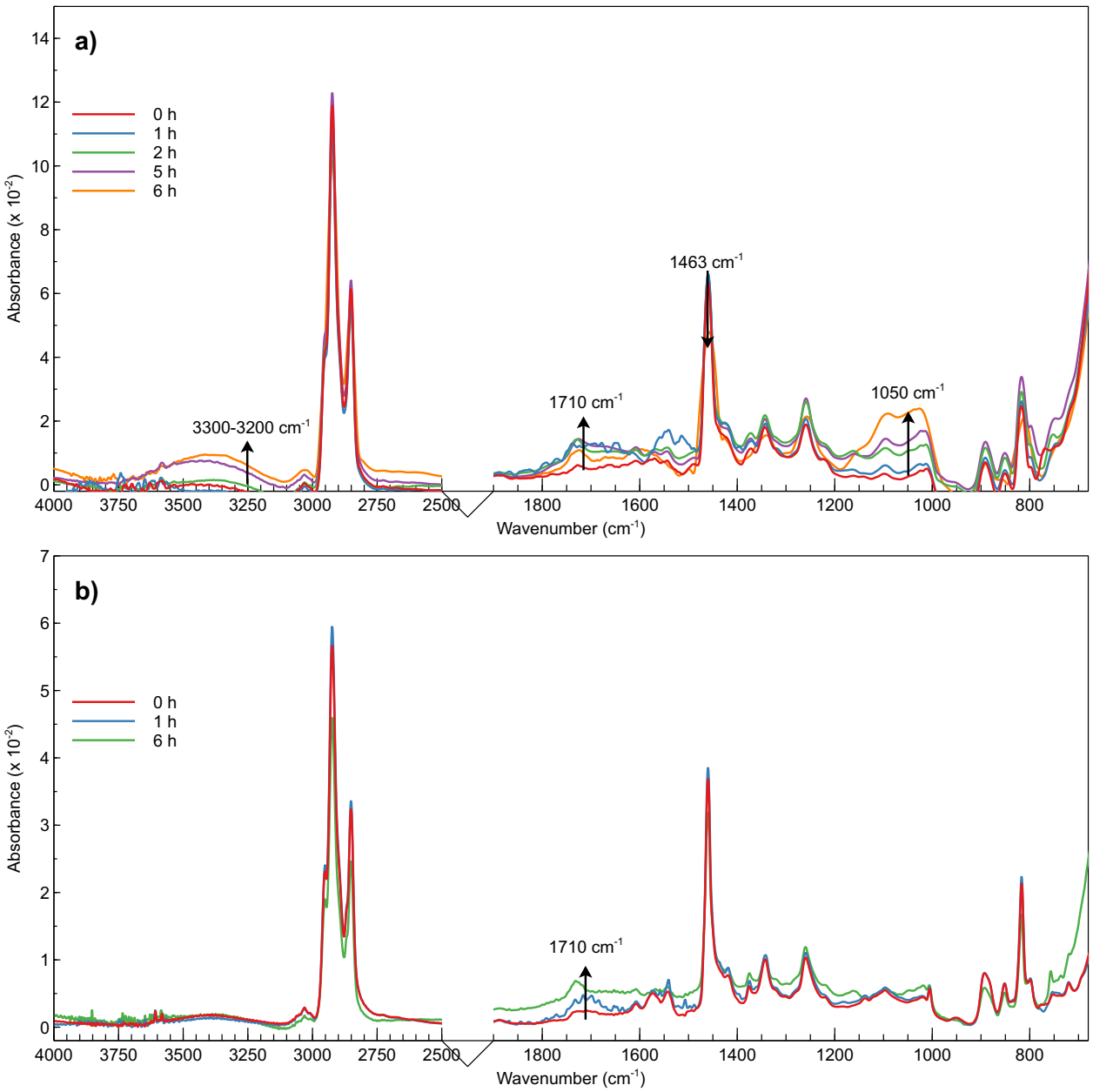

Figure S11: FTIR spectra as a function of the irradiation time (UVA light, air) of spin coated thin films of PF8BT samples: control experiment (Table 1 Entry 6) (a) and emulsion polymerized (Table 1 Entry 8) (b).

dation in inert conditions: after 6 h of testing, a negligible reduction in the maximum absorbance values have been detected. Meanwhile, the values of maximum fluorescence intensity are found to be substantially constant. Compared to the IR spectra obtained during UV-A irradiation in air, the present spectra (Figure S13) do not display significant spectral modifications.

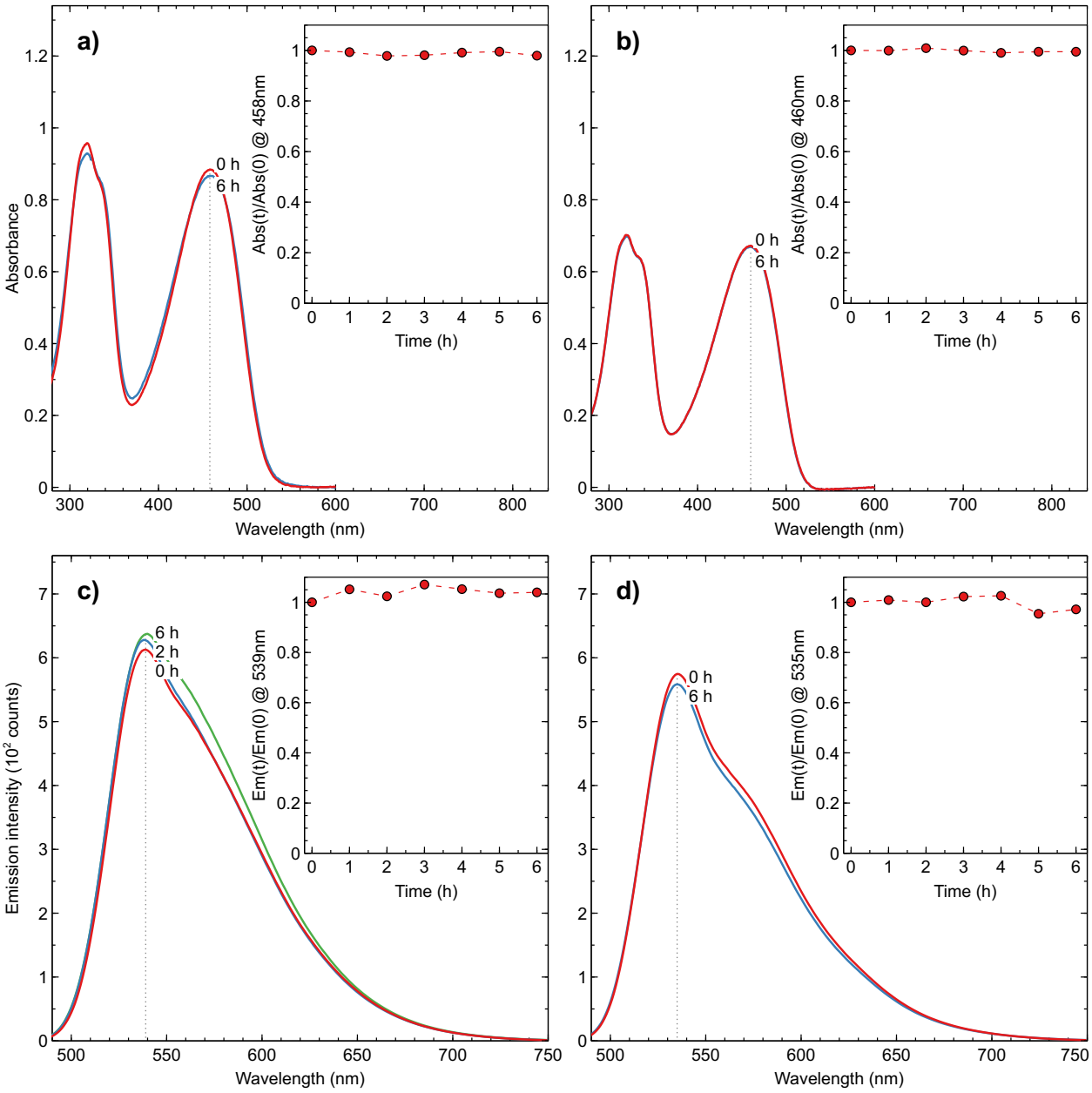

Figure S12: UV-Vis absorption (top) and steady state emission spectra under excitation at 450 nm (bottom) as the function of the irradiation time (UVA light, N_2) for spin coated thin films of of PF8BT samples: Table 1 Entry 6 (a and c) and Table 1 Entry 8 (b and d).

The outcomes of UV-Vis, fluorescence and FTIR spectroscopic analyses showed that the degradation path occurring in the samples during aging in air (non-inert atmosphere) take place more rapidly than in inert atmosphere. This suggests that photo-oxidation is responsible for the deterioration of the chemical and physical properties. Moreover, as highlighted from the results of UV-Vis, fluorescence and FTIR analyses conducted on both samples during aging in inert atmosphere, the occurrence of photolytic processes can be essentially excluded. Finally, the degradation rate of the two samples has been proven to be somewhat different. The stability of entry 8 (Table 1) resulted to be slightly higher than the one of entry 6.

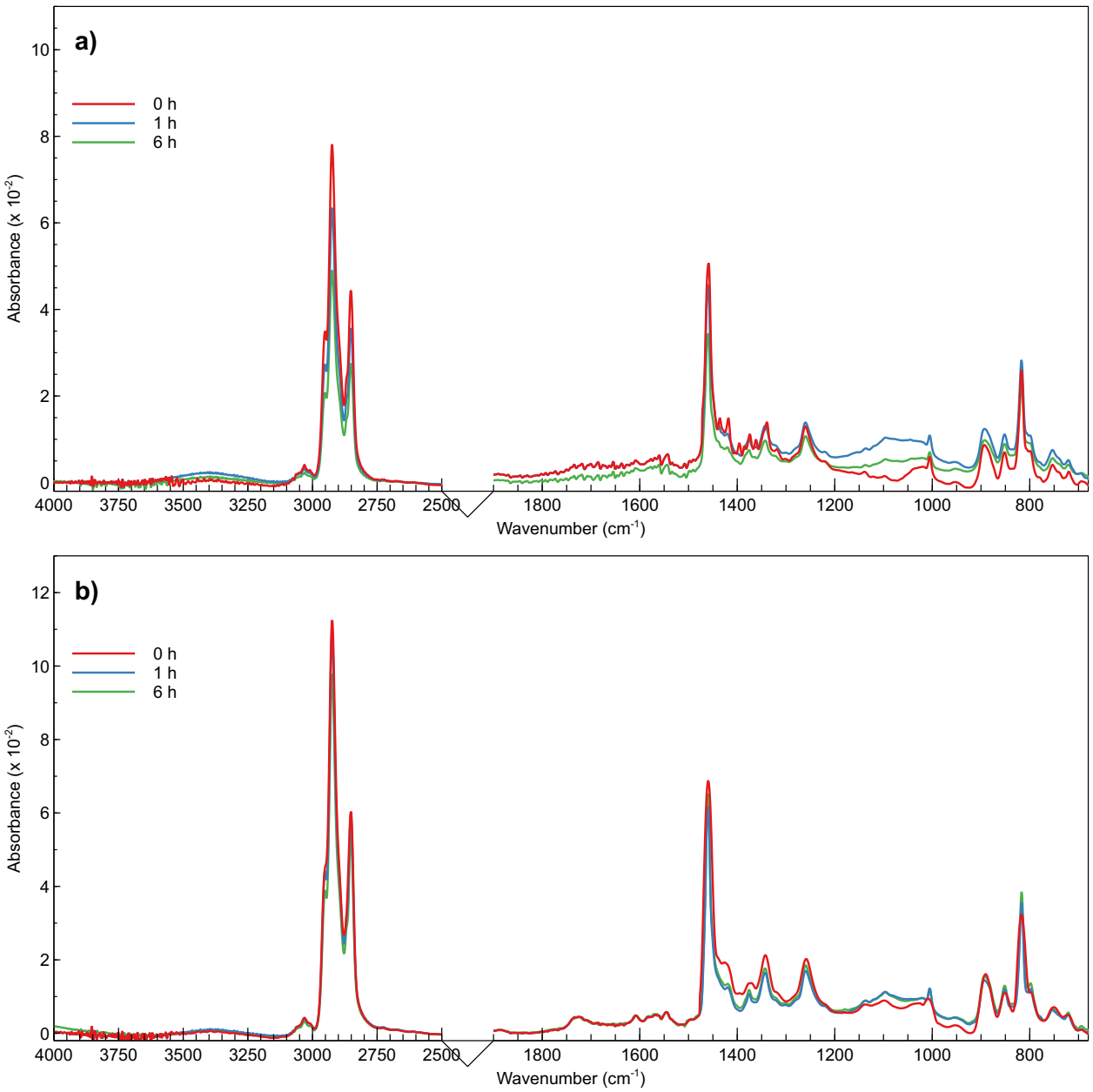

Figure S13: FTIR spectra as a function of the irradiation time (UVA light, N_2) of spin coated thin films of PF8BT samples: control experiment (Table 1 Entry 6) (a) and emulsion polymerized (Table 1 Entry 8) (b).

9 ^{1}H NMR spectra

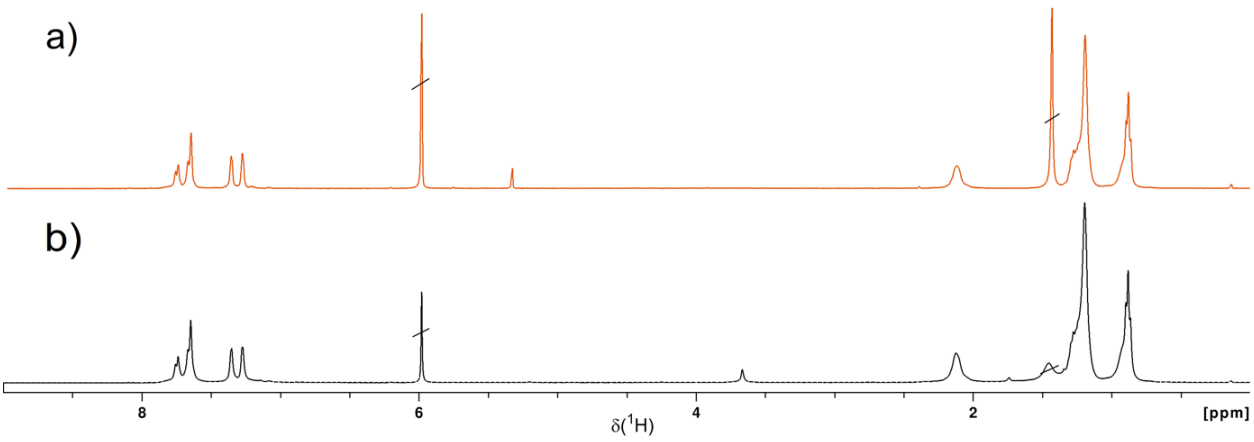

Figure S14: ^{1}H NMR of PF8T2 samples in $C_2D_2Cl_4$ at 353 K. a) table 1, entry 1; b) table 1, entry 4

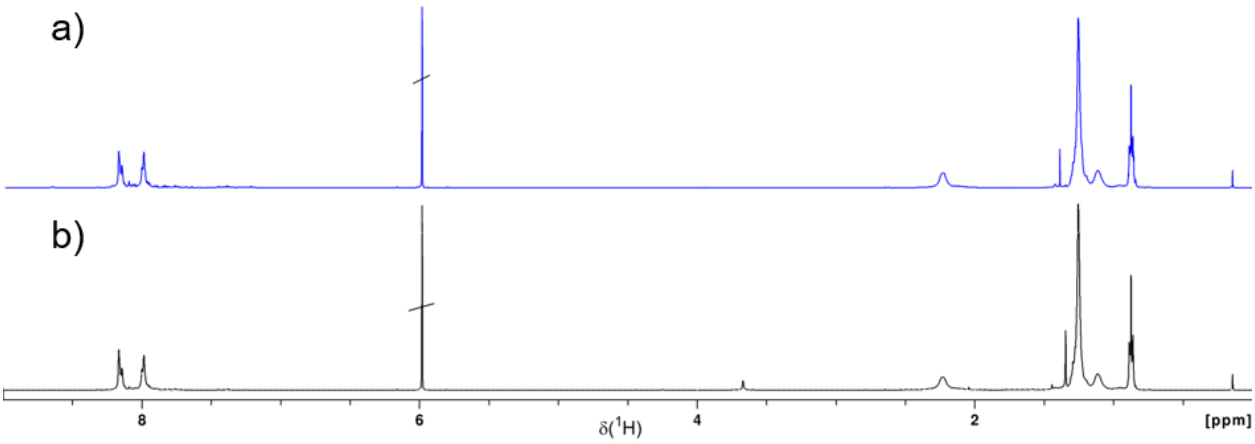

Figure S15: ^{1}H NMR of PF8BT samples in $C_2D_2Cl_4$ at 393 K. a) table 1, entry 6; b) table 1, entry 8

References

(S1) Mattiello, S.; Rooney, M.; Sanzone, A.; Brazzo, P.; Sassi, M.; Beverina, L. Suzuki–Miyaura Micellar Cross-Coupling in Water, at Room Temperature, and under Aerobic Atmosphere. *Organic Letters* **2017**, *19*, 654–657.

(S2) Gabriel, C. M.; Lee, N. R.; Bigorne, F.; Klumphu, P.; Parmentier, M.; Gallou, F.; Lipshutz, B. H. Effects of Co-solvents on Reactions Run under Micellar Catalysis Conditions. *Organic Letters* **2016**, *19*, 194–197.

(S3) Sanzone, A.; Calascibetta, A.; Ghiglietti, E.; Ceriani, C.; Mattioli, G.; Mattiello, S.; Sassi, M.; Beverina, L. Suzuki–Miyaura Micellar One-Pot Synthesis of Symmetrical and Unsymmetrical 4,7-Diaryl-5,6-difluoro-2,1,3-benzothiadiazole Luminescent Derivatives in Water and under Air. *Journal of Organic Chemistry* **2018**, *83*, 15029–15042.

(S4) Kettner, O.; Pein, A.; Trimmel, G.; Christian, P.; Röthel, C.; Salzmann, I.; Resel, R.; Lakhwani, G.; Lombeck, F.; Sommer, M.; Friedel, B. Mixed side-chain geometries for aggregation control of poly(fluorene-alt-bithiophene) and their effects on photophysics and charge transport. *Synthetic Metals* **2016**, *220*, 162–173.

(S5) Behrendt, J. M.; Guzman, J. A. E.; Purdie, L.; Willcock, H.; Morrison, J. J.; Foster, A. B.; O'Reilly, R. K.; McCairn, M. C.; Turner, M. L. Scalable synthesis of multicolour conjugated polymer nanoparticles via Suzuki-Miyaura polymerisation in a miniemulsion and application in bioimaging. *Reactive and Functional Polymers* **2016**, *107*, 69–77.

(S6) Liang, A.; Zhou, X.; Zhou, W.; Wan, T.; Wang, L.; Pan, C.; Wang, L. Side-Chain Effects on the Thermoelectric Properties of Fluorene-Based Copolymers. *Macromolecular Rapid Communications* **2017**, *38*, 1600817.

(S7) Peng, W.; Dong, J.; Li, H.-B.; Chow, C.; Hu, Q.-S. Room temperature Suzuki cross-coupling polymerizations of aryl dihalides and aryldiboronic acid/acid esters with t-Bu3P-coordinated 2-phenylaniline-based palladacycle complex as the precatalyst. *Journal of Polymer Science Part A: Polymer Chemistry* **2019**, *57*, 1606–1611.

(S8) Wang, L.; Pan, C.; Liang, A.; Zhou, X.; Zhou, W.; Wan, T.; Wang, L. The effect of the backbone structure on the thermoelectric properties of donor–acceptor conjugated polymers. *Polymer Chemistry* **2017**, *8*, 4644–4650.

(S9) Yu, F.; Wang, Z.; Zhang, S.; Ye, H.; Kong, K.; Gong, X.; Hua, J.; Tian, H. Molecular Engineering of Donor–Acceptor Conjugated Polymer/g-C3N4 Heterostructures for Significantly Enhanced Hydrogen Evolution Under Visible-Light Irradiation. *Advanced Functional Materials* **2018**, *28*, 1804512.

(S10) Zhou, X.; Pan, C.; Liang, A.; Wang, L.; Wan, T.; Yang, G.; Gao, C.; Wong, W.-Y. Enhanced figure of merit of poly(9,9-di-n-octylfluorene-alt-benzothiadiazole) and SWCNT thermoelectric composites by doping with FeCl3. *Journal of Applied Polymer Science* **2019**, *136*, 47011.

(S11) Ranger, M.; Leclerc, M. Optical and electrical properties of fluorene-based (pi-conjugated) polymers. *Canadian Journal of Chemistry* **1998**, *76*, 1571–1577.

(S12) Morin, P.-O.; Bura, T.; Sun, B.; Gorelsky, S. I.; Li, Y.; Leclerc, M. Conjugated Polymers à la Carte from Time-Controlled Direct (Hetero)Arylation Polymerization. *ACS Macro Letters* **2015**, *4*, 21–24.

(S13) Muenmart, D.; Foster, A. B.; Harvey, A.; Chen, M.-T.; Navarro, O.; Promarak, V.; McCairn, M. C.; Behrendt, J. M.; Turner, M. L. Conjugated Polymer Nanoparticles by Suzuki–Miyaura Cross-Coupling Reactions in an Emulsion at Room Temperature. *Macromolecules* **2014**, *47*, 6531–6539.

(S14) List, E. J. W.; Guentner, R.; de Freitas, P. S.; Scherf, U. The Effect of Keto Defect Sites on the Emission Properties of Polyfluorene-Type Materials. *Advanced Materials* **2002**, *14*, 374.

(S15) Liu, L.; Tang, S.; Liu, M.; Xie, Z.; Zhang, W.; Lu, P.; Hanif, M.; Ma, Y. Photodegradation of Polyfluorene and Fluorene Oligomers with Alkyl and Aromatic Disubstitutions. *The Journal of Physical Chemistry B* **2006**, *110*, 13734–13740.

(S16) Ozaki, H.; Fukushima, T.; Koshiba, Y.; Horike, S.; Ishida, K. Molecular origin of photostability for fluorene-based donor–acceptor type photovoltaic polymers. *Japanese Journal of Applied Physics* **2019**, *59*, SDDA11.

(S17) Griffini, G.; Turri, S.; Levi, M. Degradation and stabilization of poly(3-hexylthiophene) thin films for photovoltaic applications. *Polymer Bulletin* **2010**, *66*, 211–222.

(S18) Šoptrajanov, B.; Ewing, G. Infrared and Raman spectra of 1,2,5-thiadiazole. *Spectrochimica Acta* **1966**, *22*, 1417–1426.

(S19) Vasini, E. J.; Mirífico, M. V.; Caram, J. A. On experimental versus theoretically calculated properties of thiadiazole derivatives. *International Journal of Quantum Chemistry* **2011**, *111*, 1879–1884.